Original Article

Hybrid Deep Convolutional Neural Network Approach for Detecting Breast Cancer in Mammography Images

Varsha Nemade[1*], Sunil Pathak[1], Ashutosh Kumar Dubey[2]

[1]*Amity School of Engineering & Technology, Department of Computer Science & Engineering,
Amity University Rajasthan, Jaipur, India*
[2]*Chitkara University School of Engineering and Technology, Chitkara University, Himachal Pradesh, India*

[1*]*Corresponding Author : varshafegade83@gmail.com*

Abstract - Breast cancer is among the top causes of fatalities related to cancer in females. Radiologists commonly use mammogram images to detect breast tumors in their early stages. However, mammography can produce low-contrast images, making it difficult and time-consuming to segment abnormal regions. Deep convolutional neural networks (CNNs) are commonly used for image eval. This study used deep CNN models to develop a computer-aided diagnostic (CAD) system for feature extraction and classification. The proposed approach consists of three phases. In the first phase, a shallow, deep CNN model comprising five convolutional layers, five max-pooling layers, one batch normalization layer, and one dropout layer was developed and used to extract recombined images and novel features. In the second phase, the Inception-v3 model was used for label smoothing and classification due to its multiple filters with different sizes. In the third phase, features were extracted using shallow, deep CNN and Inception-v3 models. The Infallible Euclidean distance-based nonlinear dimensionality reduction approach was used to minimize dimensionality. Finally, the Gini-index-based C4.5 decision tree was used for the binary classification of mammogram images from the Digital Database for Screening Mammography (DDSM) + Curated Breast Imaging Subset of DDSM (CBIS-DDSM) and Mammographic Image Analysis Society (MIAS) datasets. The proposed hybrid shallow, deep CNN and Inception-v3 model achieved 99.52% accuracy, a 96% AUC on the DDSM + CBIS-DDSM dataset, and an accuracy of 97.53% and an AUC value of 97% on the MIAS dataset. Compared with other cutting-edge CAD systems, the proposed hybrid approach achieved higher accuracy by combining in-depth features across both datasets.

Keywords - Mammogram, Deep learning, CNN, Pre-trained, Inception-V3.

1. Introduction

Breast cancer is a cancer type that occurs commonly in women and can be life-threatening [1-5]. Therefore, early breast cancer screening and detection is crucial to provide timely and suitable treatment to minimize mortality rates [6]. Medical image analysis has proven efficient in diagnosing breast cancer [7]. Several imaging techniques, such as ultrasound, infrared thermography, magnetic resonance imaging, and digital mammography, have been employed for breast cancer prediction [8, 9]. Mammography images are used to view the breast's internal structure. [10-13], and different breast cancer indicators can be obtained from mammograms, such as architectural distortions, masses, and macrocalcifications. Among these indicators, masses and macrocalcifications are essential tumour indicators in the early stages, while architectural distortions have minimal significance [14]. Radiologists face difficulties performing manual assessments using mammogram images; therefore, CAD is employed to classify breast cancer and improve diagnostic accuracy [15, 16].

The above methods facilitate the diagnostic process and assist radiologists and physicians in decision-making. Image classification can be achieved by extracting various features from images, and machine learning (ML) has been utilized to classify breast mammogram images [14, 17, 18]. Various feature extraction techniques, such as histogram of gradients (HOG), histogram of oriented texture (HOT), grey-level co-occurrence matrix (GLCM), and Gabor wavelet transform, are available [18]. These are manual feature extraction techniques. Therefore, as an alternative, neural networks have been developed for automated feature extraction [19].

The analysis of medical images commonly employs deep learning (DL) methods [20]. DL learns features automatically from the input data and then performs image classification [21-25]. CNN are deep neural networks used for image evaluation and comprise multiple feature maps. To train CNNs from scratch, enormous computational power is required.

Moreover, the quantity of training data affects the model's efficiency. Thus, transfer learning (TL) by reusing a pre-trained model significantly saves time [26-28]. In TL networks, previous knowledge is utilized for learning new tasks, thus saving computational power and time. In TL models, there is no direct relationship between depth and model accuracy; however, accuracy depends on the dataset size (large datasets help improve the model accuracy) [29]. This work proposes a method that uses a shallow, deep CNN and a pre-trained Inception-v3 model. It performs computationally effective feature extraction and automatically identifies important features without human involvement.

Additionally, an infallible Euclidean distance-based nonlinear dimensionality reduction (IE-NDR) approach is employed in the proposed system to perform dimensionality reduction. Finally, a Gini index-based C4.5 decision tree (GI-CDT) is proposed for classifying mammogram images. GI-CDT can operate on continuous and discrete data, handle incomplete data, and provide straightforward interpretation.

The following are the significant challenges:

1. The complexity of mammogram images makes it challenging to extract useful features for classification [30].
2. Traditional feature extraction methods are manually dependent and prone to mistakes, time-consuming, and inaccurate results due to mammogram images' low contrast and wide range of breast tissue appearance [30-33].
3. Developing a computationally efficient model is challenging due to the high training time [26, 34, 35] and sizeable computational power requirements of deep models [30, 33].
4. Accurately recognizing benign and malignant masses from mammogram images is another challenge [31, 36-38].

The proposed system aims to address these challenges by combining in-depth features to reduce the limitations of current systems and aid radiologists and physicians in analyzing breast tissue structures and making decisions.

This work focused on developing a deep learning (DL) based model for the classification of mammograms. To achieve this goal, the study made several vital contributions which are as under:

1. A framework has been established based on DL architecture for categorising breast cancer. The DL model was trained to improve efficiency using data augmentation, normalization, and balancing.
2. A shallow, deep CNN model was developed with fewer layers, using transfer learning (TL) to save computational power and time. This approach was critical as developing a computationally efficient model is challenging due to the significant number of parameters involved in DL models.
3. Essential mammogram features were obtained using a deep CNN architecture through feature extraction and feature fusion processes. This helped to improve the accuracy of the model.
4. The dimensionality was reduced using IE-NDR to enhance the model's parameter interpretation and solve the overfitting problem. This approach helped in enhancing the model's generalization ability.
5. The binary classification was performed using the GI-CDT classifier to decrease impurity and uncertainty and perform better classification at each node. This approach helped to improve the accuracy of performing the classification.
6. The model's performance was evaluated on different datasets, namely the DDSM + CBIS-DDSM and MIAS datasets. It shows the approach's applicability and generalization.
7. Finally, the study compared the accuracy of different DL architectures to identify the most efficient architecture for breast mass classification.

Overall, the study made significant contributions to the development of a DL-based. The suggested model has the potential to aid radiologists and physicians in making more accurate and timely diagnoses, leading to better patient outcomes.

The remaining sections of this article are arranged as follows. Section 2 presents a literature review of manual feature extraction methods, DL detection, and classification techniques. Section 3 describes the data preparation processes and the proposed architecture process. Section 4 discusses the experimental classification results. Finally, in Section 5, the conclusions are presented.

2. Related Work

Identifying breast masses from digital mammogram images is an important research topic, and recently, ML and DL techniques have been applied in this field. Mammogram images can be processed using various algorithms to extract different features. For instance, Shastri et al. utilized a combination of HOG and HOT for feature extraction. They performed density-wise classification of mammogram patches retrieved from a medical application dataset, achieving an accuracy of over 92% [39].

Mughal et al. classified breast masses using top-hat transformation and GLCM features, which improved the classification performance by reducing the false-positivity rate [40]. Ghasemzadeh et al. proposed a DDSM model, extracting textural features with the Gabor wavelet transform, applying different classification techniques, and

achieving a mean accuracy of 0.939 [41]. Due to the variability in the size, shape, and texture of masses, there are similarities between benign and malignant masses, making diagnosis challenging [42, 43].

Kaur et al. developed a DL-based approach using k-means clustering for preprocessing and multiclass support vector machine (SVM) for classification, achieving 96.9%, 93.8%, 89.7%, and 88.7% accuracy for SVM, KNN, LDA, and DT, respectively, on images obtained from the mini-MIAS dataset [44]. Mohanty et al. designed a kernel extreme learning machine with a wrapper-based system to select essential features and predict mammogram outcomes, achieving 97.9% and 92.61% accuracy on the MIAS and DDSM datasets, respectively [45]. Yi et al. employed the GoogleNet system and an ensemble of 100 parallel networks to classify mammograms in the DDSM dataset, reporting 85% accuracy and 0.91 AUC [46].

Karthiga et al. proposed two approaches: transfer learning (TL) and a constructed CNN. They performed hyperparameter adjustments to decrease the number of parameters for training and layers, improve the feature extraction process, and increase classification performance. They achieved 95.95%, 99.39%, and 96.53% accuracy on the MIAS, DDSM, and INbreast datasets [32]. Ribli et al. introduced the Faster region-based convolutional neural networks (R-CNN) framework for object detection from mammogram images by adding a layer to create custom-designed filters. They used a CNN with 16 layers to classify detected lesions as benign or malignant and achieved an AUC of 0.85 [47].

Chougrad et al. performed multilabel image classification using a pre-trained CNN model on different mammogram datasets. They proposed a new fine-tuning strategy by applying different learning rates to each layer for learning specific features in the relevant layer. They achieved AUC values of 0.86, 0.89, 0.94, and 0.93 on the MIAS, DDSM, BCDR, and INBreast datasets [48].

Yu et al. addressed the problem of overfitting encountered during the training of deep models by extracting small parts from the region of interest (ROI). They developed two fusion models based on TL models using VGG-16 and VGG-19 and obtained accuracies of 0.8906 and 0.875%, respectively [49]. Chakravarthy and Rajaguru performed breast cancer classification using an improved crow search algorithm to select optimized parameters for extreme ML. They achieved accuracies of 98.137%, 97.193%, and 98.266% on the MIAS, DDSM, and INbreast datasets, respectively [50].

Yu et al. designed a low complexity lightweight deep CNN called DisepNet to extract features and classify breast abnormalities, achieving a mean accuracy of 95.60% [51].

Houby et al. proposed a malignant and nonmalignant classification of breast masses. They preprocessed the data by removing noise, enhancing images, determining the ROI, augmenting data to manage data imbalance, and resizing images. They used a CNN model with small filter sizes to save computational power and achieved an AUC of 0.945, 0.924, and 0.946 on the MIAS, DDSM, and INbreast datasets, respectively [52].

Saber et al. applied segmentation to extract affected patches, reducing training time. They used pre-trained CNN models such as VGG19, VGG16, Inception-v2, ResNet, Inception-v3, and ResNet50 for identifying breast cancer from images in the MIAS dataset and achieved 98.96% accuracy by applying the 80–20 method and 10-fold cross-validation [53].

Malebary and Hashmi employed boosting, CNNs, random forests, recurrent neural networks (RNNs), and K-means clustering to increase accuracy. They addressed issues related to the semantic features of images and the extraction of patches in low-contrast images. The authors achieved 95% and 96% accuracies on the MIAS and DDSM datasets, respectively [54].

Kulkarni et al. used various CNN architectures on different mammogram datasets. They evaluated the performance on smaller datasets and classified breast masses into malignant or benign using DenseNet with data augmentation, achieving 99.91% accuracy [55]. Oyetade et al. employed an improved deep CNN (DCNN) with fuzzy-SVM (FSVM) to classify mammogram images into three classes (normal, benign, and malignant) and two classes (benign and malignant). They achieved 81.43% and 85% accuracy for the three-class classification on DDSM and CBIS-DDSM datasets, respectively, and 86.6% and 93% for the two-class classification on DDSM and CBIS-DDSM datasets, respectively [56].

Haq et al. developed a DCNN using the feature fusion approach to identify mammogram abnormalities and classify them into regular and cancerous. They achieved an accuracy of 0.994 on the MIAS dataset [57, 58]. Mohapatra et al. utilized pre-trained weights and training from scratch to perform multi-class classification on the mini-DDSM dataset using CNN architectures, including VGG16, AlexNet, and ResNet50. They achieved 65%, 65%, and 61% accuracy for AlexNet, VGG16, and ResNet50, respectively [59].

Houssein et al. employed a hybrid CNN with an improved marine predator's algorithm (IMPA) optimization algorithm to detect abnormalities in breast masses. They used IMPA to get the best hyperparameters of the pre-trained model ResNet50 and achieved 98.32% and 98.88% accuracies on the CBIS-DDSM and MIAS datasets, respectively [60, 61]. Song et al. developed a CAD model for

mammogram classification on the DDSM datasets by extracting features using GoogleNet and Inception-v2 and manual feature extraction using GLCM and HOG. Features were classified using XGBoost and achieved an accuracy of 92.8% [11]. Khan et al. used CNN architectures such as GoogleNet, VGGNet, and ResNet-50 to extract features and achieved an accuracy of 97.67% [62]. After reviewing the literature, it is evident that there is a demand for a model that can perform multiple tasks with automated feature extraction. Additionally, there is a necessity for a model that requires minimal computational power and avoids overfitting.

3. Methodology

We have developed a DL-based framework for classifying breast lesions from mammogram images. The proposed architecture uses a shallow, deep CNN and a pretrained Inception-v3 model. Figure 1 depicts the different architectures utilized in our framework. Specifically, Figure 1a shows the shallow, deep CNN architecture, Figure 1b shows the architecture of the pretrained Inception-v3 model, and Figure 1c illustrates our proposed architecture for feature extraction using a combination of the shallow, deep CNN and Inception-v3 models, in addition to dimensionality reduction and classification. The major components of the proposed architecture are as follows:

3.1. Datasets and Preprocessing

We have used two mammogram datasets for the experiments.

3.1.1. DDSM and CBIS-DDSM Datasets

The DDSM and CBIS-DDSM (updated DDSM) mammography datasets were utilized in this study. Both datasets consist of both positive and negative images. Positive images correspond to individuals with cancer, while negative images represent healthy individuals. The CBIS-DDSM dataset contains images of masses or calcifications and images from the DDSM dataset without any anomalies. CBIS-DBSM has 55,890 images containing patches of extracted ROI of size 299×299. The negative images from DDSM were tiled into 598×598 squares and then downsized to 299×299 squares.

A small amount of padding and masks were used to extract ROIs from the positive (CBIS-DDSM) images. Subsequently, three 598×598 images were randomly generated by cropping each ROI, and those images were then randomly rotated and flipped. Two labels were used: 0 for negative and 1 for positive cases; 86% of the images are negative, whereas 14% are positive.

This dataset is available on Kaggle [63] as TFRecords. The TensorFlow library was used to transform all images extracted from the TFRecords format to the .jpg format. Normalization was performed on the entire image to preserve

a uniform range across all pixels and prevent bias. This dataset is highly unbalanced; thus, we oversampled the minority class.

3.1.2. MIAS Dataset

A UK research group organization created the MIAS dataset for the research purpose. MIAS has 322 digitized films with a truth mark by radiologists indicating the places of potential abnormalities; 208 of these images are considered normal, 68 are benign, and 54 are cancerous. These images were described by radiologists as follows: architectural distortion (19 cases), speculated masses (15 cases), microcalcification (30 cases), circumscribed masses (25 cases), and bilateral asymmetry (15 cases). This study lowered this dataset to a 200-micron pixel, and clipping was performed so that every image was 1024×1024 pixels [64]. The labels used were 0 for benign and 1 for malignant. Flipping, rotation, and resize operations were applied to generate more images on the MIAS dataset.

3.2. CNN Architecture
3.2.1. Shallow Deep CNN

We implemented a shallow, deep CNN comprising five convolutional, five max-pooling, a dropout and batch normalization layers. Figure 2 illustrates the architecture of shallow, deep CNN. The convolutional layers perform dot-product operations between learnable parameters called kernels and the input image. The kernel size of every convolutional layer is 3×3 with different filters. The down-sampling operation is done by the max-pooling layers on earlier layers to decrease the quantity of computing needed; the size of the max-pooling layers is 2×2.

Fully connected (FC) layers display the complete links to all the neurons in the last layer. The previous layer output normalizes by the batch normalization layer. The dropout layer is used to minimize overfitting. Lastly, flattening and dense layers are used. We employed the rectified linear unit (ReLU) activation function to the middle layers, while for the output layer, we used the sigmoid function. We selected the Adam optimizer and binary cross-entropy as the loss function because the Adam optimizer offers a faster computational time and requires less parameter tuning than other optimization algorithms.

3.2.2. Inception-V3 Architecture

Compared to other architectures, the traditional Inception model has more layers but requires fewer parameters to be trained. It has a deep network with tunable blocks and convolutional filters ranging from 5×5 to 1×1n cascade. Inception-v3 has fewer parameters due to the factorization of more extensive convolution layers. Through changes in the original structure, Inception-v3 can also be used for small datasets [65]. The Inception-v3 [66] model can recognize 1000 classes due to its training on ImageNet datasets.
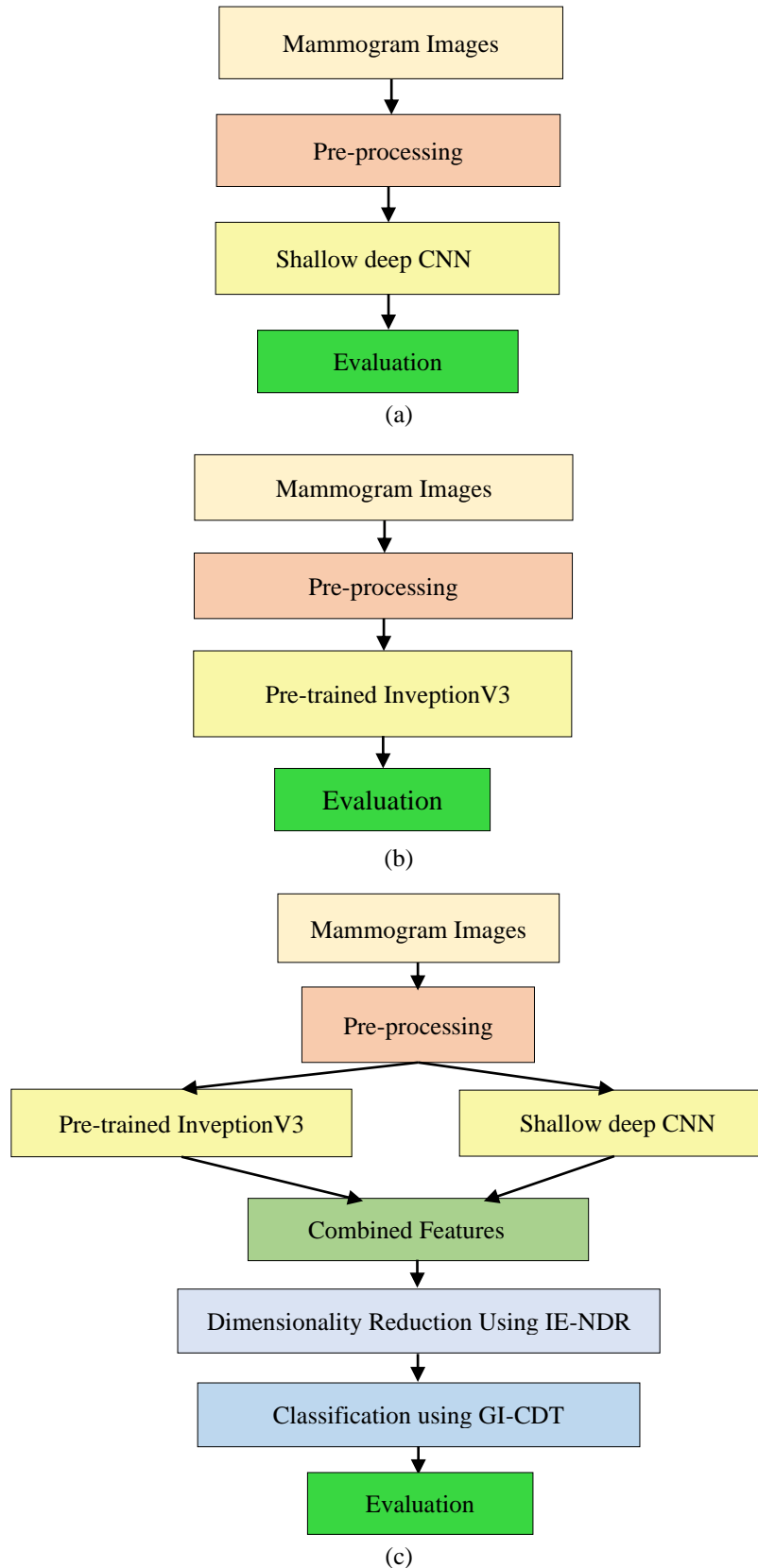
Fig. 1 a) Shallow, deep CNN b) Inception-V3 c) Proposed architecture
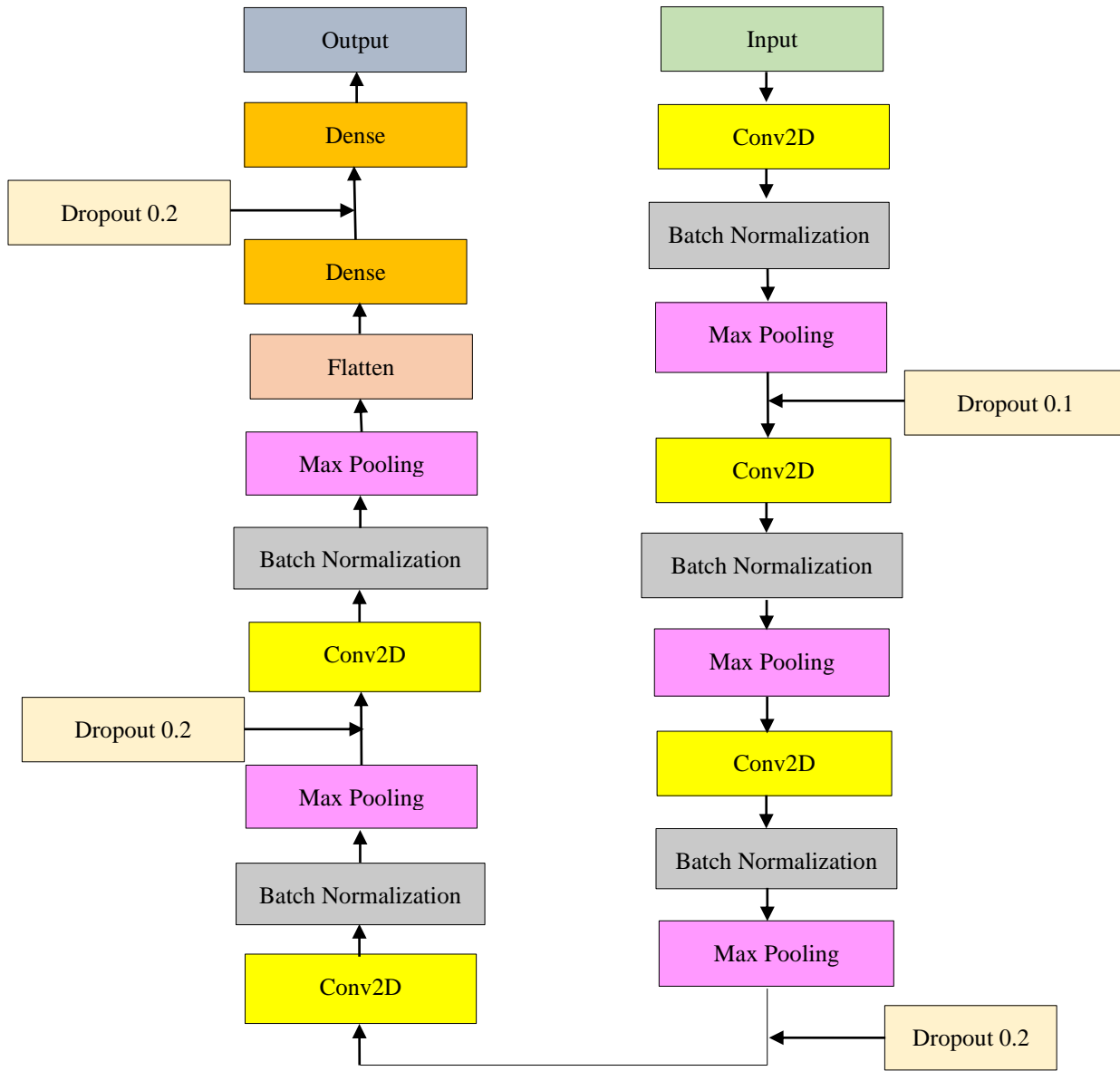
Fig. 2 Shallow, deep CNN architecture

The error rate for the top-5 is 3.5%, whereas that for the top-1 is 17.3%. In this study, we added an FC layer to flatten the output of the previous layers and a dropout layer to reduce overfitting. We used the sigmoid function in the output layer, and the remaining ReLU function was used. In addition, the Adam optimizer with the binary cross-entropy loss function is used.

3.2.3. Feature Extraction

For performing the classification of mammogram images, the features must be extracted. We extracted features using the proposed hybrid shallow, deep CNN and pre-trained Inception-v3 CNN model. In the shallow, deep CNN model, removing the output layer and extracting features

were performed. In the pre-trained Inception-v3 model, all the layers except the output layer were removed, and features were extracted. Finally, the features extracted using the shallow, deep CNN and pretrained Inception-v3 CNN model were combined.

3.3. Dimensionality Reduction using Infallible Euclidean Distance-Based Nonlinear Dimensionality Reduction (IE-NDR)

The features extracted using the shallow, deep CNN and Inception-v3 architecture were combined. IE-NDR was used to convert high-dimensional data into lower-dimensional data for dimensionality reduction. The flowchart of the proposed IE-NDR algorithm is shown in Figure 3.
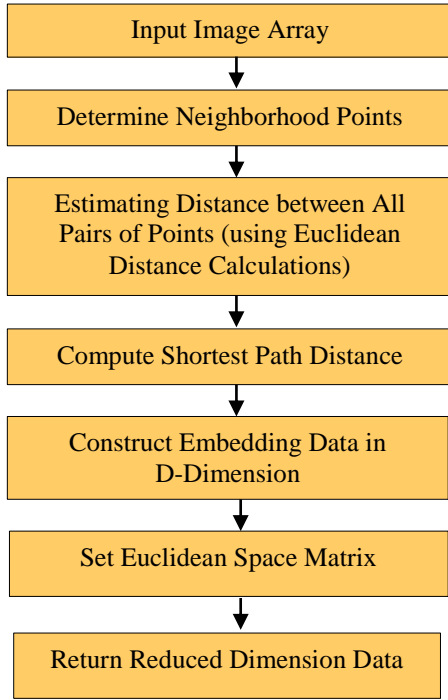
Input Image Array

↓

Determine Neighborhood Points

↓

Estimating Distance between All Pairs of Points (using Euclidean Distance Calculations)

↓

Compute Shortest Path Distance

↓

Construct Embedding Data in D-Dimension

↓

Set Euclidean Space Matrix

↓

Return Reduced Dimension Data

Fig. 3 IE-NDR working flow

3.3.1. Infallible Euclidean Distance

Due to its efficiency and simplicity, Euclidean distance is widely used in image recognition algorithms and for image distance measurement. Assume E and R as two images of size $M \times B$, $E = (E\_11, E\_12, \ldots, E\_SB)$, $R = (R\_11, R\_12, \ldots, R\_SB)$, $(I = 1, 2, \ldots, S, j = 1, 2, \ldots B)$ conventional Euclidean distance,

$$\text{dist}(E, R) = \left[\sum_{a=1, b=1}^{S,B}(E_{ab} - R_{ab})^2\right]^{\frac{1}{2}},$$

and E_{ab} and R_{ab} representing E and R, respectively.

The conventional Euclidean distance only measures the variance of the corresponding two image pixels; however, when the image is slightly distorted or shifted, a high Euclidean distance is obtained, and errors might occur when measuring the image similarity. The coefficient matrix for infallible Euclidean distance measurement can be expressed as follows (Equation 1):

Coefficient Matrix Λ:Λ

$$= \begin{bmatrix} A_{11} & \cdots & A_{1b} & \cdots & A_{1N} \\ \vdots & \ddots & \vdots & \ddots & \vdots \\ A_{a1} & \cdots & A_{ab} & \cdots & A_{aN} \end{bmatrix} . A_{ij}$$

$$\begin{matrix} \vdots & \ddots & \vdots & \ddots & \vdots \\ A_{M1} & \cdots & A_{Mb} & \cdots & A_{MN} \end{matrix} \quad , \quad (1)$$

where A_{ij} represents the function $(A_{aj} = f(|P_a - P_b|)$ related to the distance between the pixels, and $|P_a - P_b|$ is the relative distance among the coordinates of ath and b^{th} pixels. The infallible Euclidean distance can be obtained using Equations 2 and 3:

$$dist^2(E, R) = \sum_{a=1, b=1}^{S,B} F_{aj}(E' - R')(E' - R') \qquad (2)$$

$$= (E - R)^T \Lambda (E - R). \qquad (3)$$

It has been discussed in complete exploration through Algorithm 1. More compact feature representation reduces the computational complexity. As such, the combined feature dimension was reduced using IE-NDR (Algorithm 2).

3.4. Classification of Breast Cancer by using GI-CDT
3.4.1. Gini Index (GI)

GI is a statistical inequality index used for fault diagnosis. It is more effective compared with kurtosis and correlation in detecting repetitive signals. GI values are in the range of [0, 1] and exhibit higher sensitivity in differentiating between lower and higher values. The GI value can be obtained as follows (Equation 4):

$$GI(x) = 1 - 2\sum \frac{|x_{[k]}|}{x_i} \times \left[\frac{B - k + \frac{1}{2}}{B}\right] \qquad (4)$$

Where, $x = [x(1), \ldots, x(B)]$ with its element reordered and represented by $x_{[k]}$

For $k = 1, 2, \ldots \ldots B$, where $x1$ is the $I1$ norm of x and

$$|x_{[1]}| \leq |x_{[2]}| \leq, \ldots \ldots \ldots \leq |x_{[B]}| \qquad (5)$$

3.4.2. C4.5 Decision Tree Classifier

For effective classification, in this study, the C4.5 DT classification algorithm was used because DT can produce recognizable rules, implement classification without any need for computation, manage categorical and continuous variables, and afford a clear representation of the relevant essential areas for prediction and classification. C4.5 DT produces a DT by learning from the training set.

For C4.5 DT, the gain ratio is measured as shown in Equations (6) and (7):

$$\text{gain ratio}(e) = \frac{\text{gain}(e)}{\text{split info}(e)} \qquad (6)$$

with

$$\text{split info}(e) = \sum_{b}^{m} \frac{|S_b|}{|s|} \log_2\left(\frac{|S_b|}{s}\right) \qquad (7)$$

Algorithm 1: Infallible Euclidean distance

Step 1: Measure the Euclidean distance for all features in each class.
For class I and j for 'A' feature is,

$$E_{a,b}^{fA} = d(D_a^A, F_b^A) = \sqrt{\sum_{k=1}^{n} (D_{ka}^A - D_{kb}^A)^2}$$

n = no. of samples containing every class

Step 2: M matrix of size $(W \times \frac{(w-1)}{2} \times T)$ generate by presenting a one-one rule for all features in each class.

$$E \quad \Lambda: \Lambda = \begin{bmatrix} D_{11} & \cdots & D_{1b} & \cdots & D_{1B} \\ \vdots & \ddots & \vdots & \ddots & \vdots \\ f_{a1} & \cdots & F_{ab} & \cdots & F_{aB} \\ \vdots & \ddots & \vdots & \ddots & \vdots \\ D_{S1} & \cdots & D_{Sb} & \cdots & D_{SB} \end{bmatrix} \quad (\text{ } (W \times ((w-1))/2 \times T)$$

The total number of classes and features are w and z correspondingly. Feature numbers are $f_1, f_2, \ldots \ldots f_T$ of $1, 2, \ldots, z$ respectively. $(W \times \frac{(w-1)}{2} \times T)$ is considered as total Euclidean distance class combinations.

Step 3: Measure the Euclidean distance between every matrix feature M,
$a^{th} - b^{th}$ class combinations of matrix S,

$$e_{a,b}^{fA.fB} = d(f_{ab}^A, f_{ab}^B)_S = |E_{ab}^{fA} - E_{ab}^{fB}|_S$$

$$\begin{bmatrix} e_{1,2}^{f_1,f_2} & e_{1,2}^{f_1,f_3} & \cdots & e_{1,2}^{f_{T-1},f_T} \\ \vdots & \vdots & \ddots & \vdots \\ \vdots & \vdots & \ddots & \vdots \\ e_{(w-1),w}^{f_1,f_2} & e_{(w-1),w}^{f1,f3} & \cdots & e_{(w-1),w}^{f_{T-1},f_T} \end{bmatrix} - (W \times \frac{(w-1)}{2}) \times (T \times \frac{(T-1)}{2})$$

$(T \times \frac{(T-1)}{2})$ is the obtained combination of total features.

Step 4: Calculate the size of the vector and mean as $\left(T \times \frac{(T-1)}{2}\right)$

$$p = [Ed^{f_1f_2} \quad Ed^{f_1f_3} \ldots \ldots Ed^{f_{T-1}f_T}] 1 \times \left(T \times \frac{(T-1)}{2}\right)$$

The index vector is p, $I_{a,b}$ is an index among a^{th} and b^{th} feature

Step 5: Arrange the vector p, from higher to lower mean value along with the index,

$$Q1 = \left[Is_{a,b}^1 \quad Is_{a,b}^2 \ldots \quad Is_{a,b}^{\left(T \times \frac{(T-1)}{2}\right)}\right] 1 \times \left(T \times \frac{(T-1)}{2}\right)$$

Q1 is a sorted index. This index is re-arranged concerning Q among a^{th} and b^{th} feature.

Step 6: Separate I and J feature index value from Q1

$$I = \left[a1 \quad a2 \quad \ldots \quad a\left(\frac{T \times (T-1)}{2}\right)\right]_{1 \times \left(T \times \frac{(T-1)}{2}\right)}$$

$$J = \left[b1 \quad b2 \quad \ldots \quad b\left(\frac{T \times (T-1)}{2}\right)\right]_{1 \times \left(T \times \frac{(T-1)}{2}\right)}$$

Step 7: Combine the feature index vector I and J,
Arrange the feature index as per Vector R

$$R = \left[a1\ b1\ a2\ b2\ \ldots\ \ldots . a\left(\frac{T \times (T-1)}{2}\right)\ b\left(\frac{T \times (T-1)}{2}\right)\right]_{1 \times (z \times (z-1)))}$$

Step 8: according to index Vector V, feature ranking (U) is,

$$U = [D_{S1}\ \ D_{s2}\ \ldots .. D_{sT}]_{(1 \times T)}$$

$D_{s1}, D_{s2}, \ldots \ldots . D_{sT}$ are the features ranked as 1,2, …, T correspondingly.

Algorithm 2: IE-NDR

Input: matrix $A = \left[A^{(1)}, \ldots .. A^m\right] \in R^n \times \sum_{a=1}^{m} k_a$, k is the dimension of the basis matrix B, the initial value of B is B°

$$= [I_k, 0]'.$$

Output: The low $-$ dimensional optimal consensus representation B.

$$T = 0.$$

Using this $E_{a,b}^{fA} = d\left(D_a^A, F_b^A\right) = \sqrt{\sum_{k=1}^{n}\left(D_{ka}^A - D_{kb}^A\right)^2}$ We measure Euclidean distance among the class.

Perform singular value decomposition of matrix $E = A.(P^z)'$ and obtain $E = U\Delta V$

$B^{z+1} = UV$

$z = z + 1$

Until there is no change to B

Algorithm 3: c4.5 Decision tree classifier

1. Create a $node\ B$,
2. If S Tuples belong to the same single class(C), then B is returned as leaf-node been labelled as $class\ C$
3. if at_{list} seems empty, then B is returned to be leaf-node, which is labelled with the primary class within S.
4. $Attribute\_selection\_method(S, at_{list})$ is applied to determine the best and most effective splitting -criterion;
5. Node B is labelled with that splitting criterion;
6. if the attribute (splitting one) seems to be discrete-valued and permits multi-day splits, then define at_{list}
7. If utilised C4.5 classification algorithm, then the gain ratio ought to be calculated,
8. $gain\ ratio(e) = \frac{gain(e)}{split\ info(e)}$ With $split\ info(e) = \sum_b^m \frac{|S_b|}{|s|} \log_2\left(\frac{|s_b|}{s}\right)$
9. For every outcome b of the above splitting criteria, let the set of data tuples in S is represented by S_b that satisfies node b outcome.
10. if S_b depicted as empty then labelled lead is attached with high majority-class within S to B node.
11. else the node is attached, which is obtained through generate-decision-tree$(S_b\ at_{list})$ to node B;
12. return B;

The C4.5 DT classifier algorithm is described in Algorithm 3. GI-CDT considers all possible outcomes of a decision and traces each path to a conclusion. It performs a comprehensive analysis of the results along each branch and identifies decision nodes that need further analysis. GI-CDT builds several trees from a single dataset and selects the best decision among the forest of trees. It improves the ID3 algorithm by dealing with continuous and discrete attributes and pruning trees after construction. The workflow of GI-CDT is shown in Figure 4.

4. Results

We conducted experiments on two mammography datasets, DDSM + CBIS-DDSM and MIAS. Our experiments involved binary classification of positive or negative cases on both datasets, with 80% of images used for training and 20% for testing. We used five-fold cross-validation for evaluation, running 100 epochs with a batch size 32. The experiments used Python 3.7 in Google Colab Pro, utilizing an online GPU and 16-GB RAM. TensorFlow and Keras were used as backend libraries. To measure the

performance of the models, we evaluated accuracy, sensitivity, specificity, precision, recall, and ROC curve, enabling us to conduct a comparative analysis.

Accuracy: It quantifies the rate of accurate classification and is expressed as follows:

$$\text{Accuracy} = \frac{\text{True Negative+True Positive}}{\text{True Negative+False Negative+True Positive+False Positive}} \quad (8)$$

Sensitivity**:** It is the ratio of positive segments recognized correctly and is expressed as follows:

$$\text{Sensitivity} = \frac{\text{True Positive}}{\text{True Positive+False Positive}} \quad (9)$$

Specificity: It is the ratio of negative segments recognized correctly and is expressed as:

$$\text{Specificity} = \frac{\text{True Negative}}{\text{True Negative+False Negative}} \quad (10)$$

Precision: Precision is a measure of the number of correct classifications, and it is written as

$$\text{Precision} = \frac{\text{True Positive}}{\text{False Positive+True Positive}} \quad (11)$$

Recall: It is the proportion of relevant and retrieved images to the number of relevant images, and it is represented as.

$$\text{Recall} = \frac{\text{rel image} \cap \text{ret image}}{\text{rel image}} \quad (12)$$

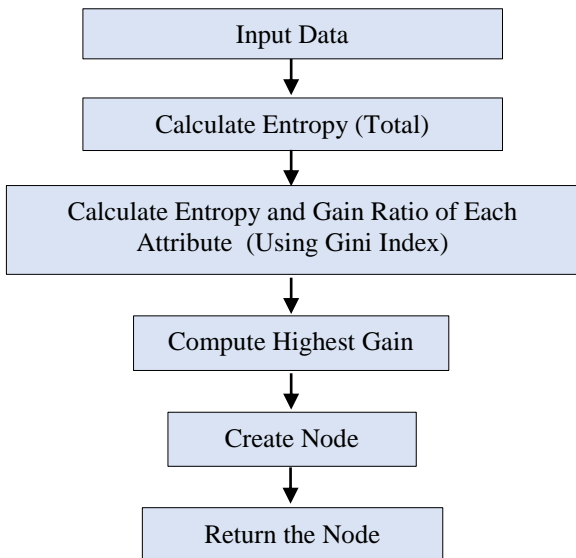Where, "rel" stands for "relevant," "ret" stands for "retrieved,".

Fig. 4 Workflow of GI-CDT

ROC: It represents receiver operating characteristics. It is measured by putting the number of actual favourable rates against the number of false favourable rates for the individual classifiers at different thresholds. The following part describes the experiments' results for the DDSM + CBIS-DDSM and MIAS datasets.

4.1. DDSM + CBIS-DDSM Dataset
In our experimentation, we utilized the DDSM + CBIS-DDSM dataset, which includes two views (craniocaudal and mediolateral-oblique) and already-segmented images. Figure 5 and Figure 6 illustrate the performance metrics achieved on the DDSM + CBIS-DDSM dataset. In the first experiment, we employed an end-to-end shallow, deep CNN model on unseen data from the dataset, achieving an accuracy, sensitivity, and specificity of 97.99%, 97.59%, and 98.4%, respectively. We used a pre-trained Inception-v3 model in the second experiment, modifying the output layer. On the dataset's unseen data, this model achieved an accuracy, sensitivity, and specificity of 96.07%, 95.52%, and 99.63%, respectively.

The shallow, deep CNN model required less training time than the pre-trained Inception-v3 model (Table 1) and achieved higher accuracy. In the third experiment, a feature set was created. These features combined the features generated using our shallow, deep CNN and the pre-trained Inception-v3 model. The shallow, deep CNN model and Inception -v3 produced 128 and 1000 features, respectively. A single feature vector with 1128 features was created by combining these features. We used IE-NDR to minimize the feature space and the classification process complexity. Finally, for classification, GI-CDT was used. Figure 7 shows the feature space classification results. We minimized the number of features to 30, 40, 50, 60, 70, 80, 90, and 100 and achieved an accuracy of 99.41%, 99.52%, 99.51%, 99.46%, 99.41%, 99.42%, 99.40%, and 99.39%, respectively. For 40 features, we achieved the highest accuracy for the proposed architecture.

4.2. MIAS Datasets
In the MIAS dataset, image augmentation was performed to generate more images, and then binary classification (benign and malignant) was performed. In addition, three experiments were performed on this dataset, and the results were evaluated. Figure 8 and Figure 9 compare different performance indicators on the MIAS dataset. In the first experiment on the MIAS dataset, an end-to-end shallow, deep CNN was applied. This model was used on the dataset's unseen data, and accuracy, sensitivity, and specificity of 95.53%, 98.19%, and 96.9%, respectively, were achieved. In the second experiment, a pre-trained Inception-v3 model was used by changing the output layer. This model was used on the dataset's unseen data, and accuracy, sensitivity, and specificity of 89.32%, 87.91%, and 90.6%, respectively, were achieved.

The designed shallow, deep CNN model achieved higher accuracy than the pre-trained Invection-v3 model; moreover, the training time of the shallow, deep CNN model was less than that of the pre-trained Invection-v3 model (Table 2). In the third experiment, we constructed a feature set for the MIAS dataset using the same approach as that used for the DDSM + CBIS-DDSM dataset. We then utilized IE-NDR to reduce the large dimensions of the generated feature set and classified the reduced set using GI-CDT. Figure 10 presents the classification results based on the feature space. We reduced the number of features to 30, 40, 50, 60, 70, 80, 90, and 100, achieving accuracies of 97.33%, 97.53%, 97.00%, 97.00%, 99.31%, 97.40%, 97.31%, and 99.37%, respectively. The proposed architecture achieved the highest accuracy on the MIAS dataset with 40 features.

The figures in Figure 11 and Figure 12 depict the ROC curves for all three experiments conducted on both datasets. On the DDSM + CBIS-DDSM dataset, the AUC values for the three experiments were 0.98, 0.95, and 1.00, respectively. The proposed architecture that combined features had a higher AUC value than other DDSM + CBIS-DDSM dataset architectures. On the other hand, the AUC values for the three experiments conducted on the MIAS dataset were 0.98, 0.89, and 0.97, respectively. The shallow, deep CNN designed in this study had a higher AUC value than other architectures on the MIAS dataset. The effectiveness of the proposed system was compared with existing systems, and the results are shown in Table 3.

The comparison demonstrated that our system outperformed the competing systems. For example, Gnanasekaran et al. designed a CNN model that achieved an accuracy of 92.54% on the MIAS dataset, whereas our shallow, deep CNN achieved an accuracy of 97.53%. Our system's accuracy on the MIAS dataset was also higher than the models developed by Houby et al. [52] and Karthiga et al. [32]. Ragab et al. [67] used AlexNet, GoogleNet, ResNet-18, ResNet-50, and ResNet-101 to extract and classify in-depth features, achieving 97.40% accuracy on the MIAS dataset. Our system yielded slightly higher accuracy on the MIAS dataset, but the AUC value obtained using our system was slightly lower than that obtained by Ragab et al. Furthermore, the system proposed in this study achieved higher accuracy on the DDSM + CBIS-DDSM dataset than the improved CNN model developed for end-to-end training by Kumar et al. [68-70].

Table 1. Training time on the DDSM + CBIS-DDSM dataset

Model	Training Time(min)
Shallow deep CNN	Approx. 13-14 min for each fold
Pre-trained InceptionV3	Approx. 18-19 min for each fold

Table 2. Training time on the MIAS dataset

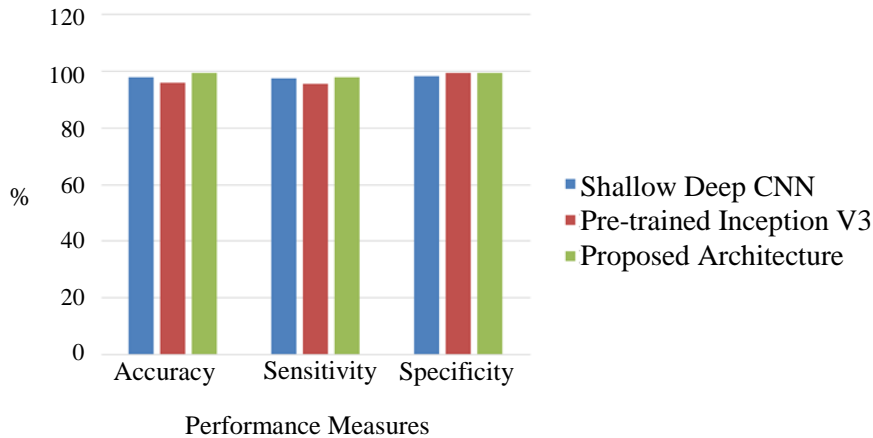| Model	Training Time(min)
Shallow deep CNN	Approx. 3-4 min for each fold
Pre-trained InceptionV3	Approx. 5-6 min for each fold

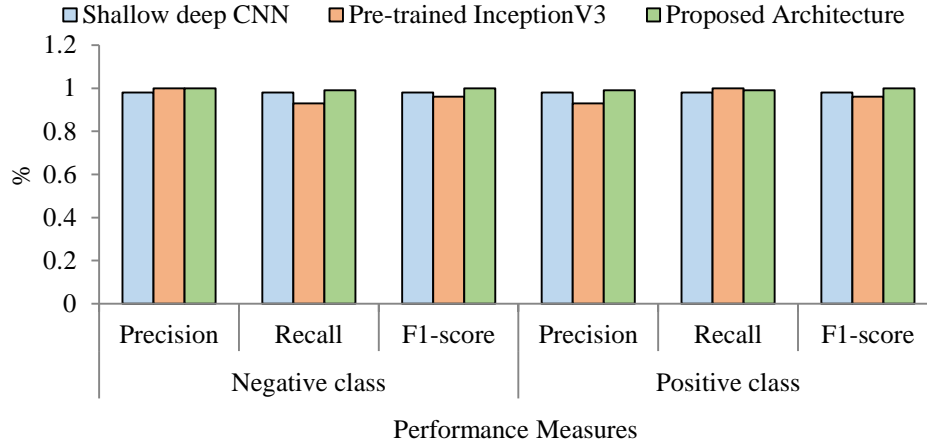**Fig. 5 Accuracy analysis for the DDSM + CBIS-DDSM dataset**

Fig. 6 Class-wise performance measurement for different experiments on the DDSM + CBIS-DDSM dataset
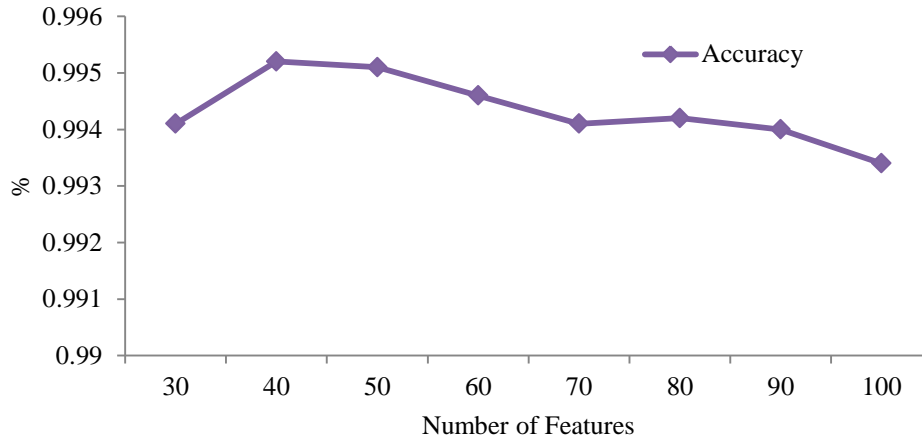

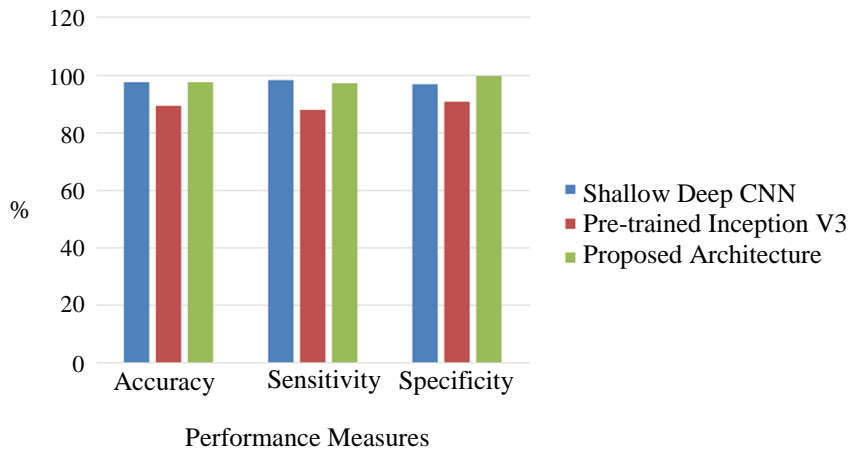**Fig. 7 Comparison of combined features accuracy on the DDSM+ CBIS-DDSM dataset**

Fig. 8 Accuracy analysis for the experiments on the MIAS dataset
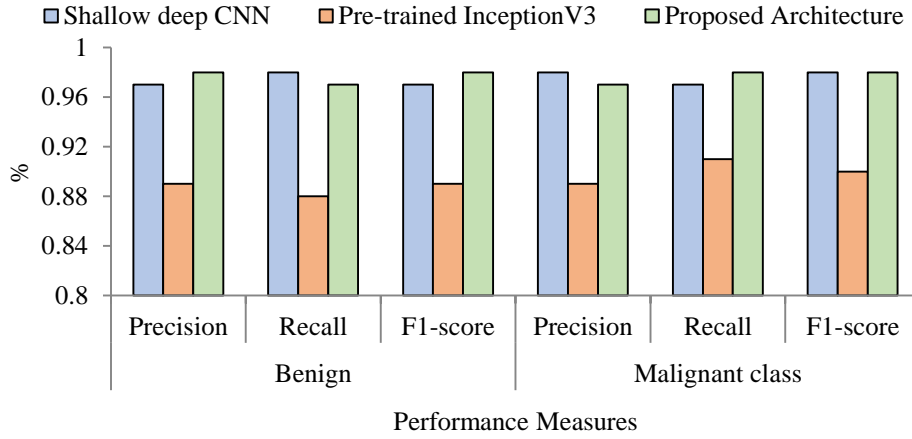
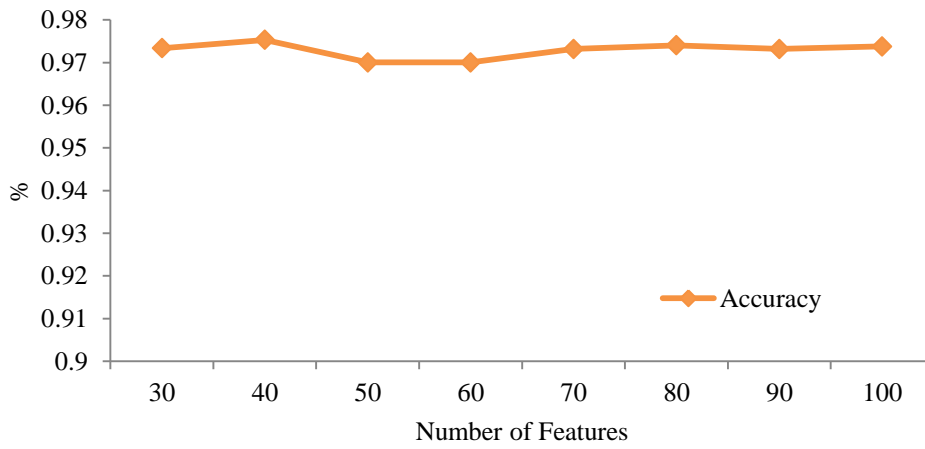**Fig. 9 Class-wise performance indicators for different experiments on the MIAS dataset**

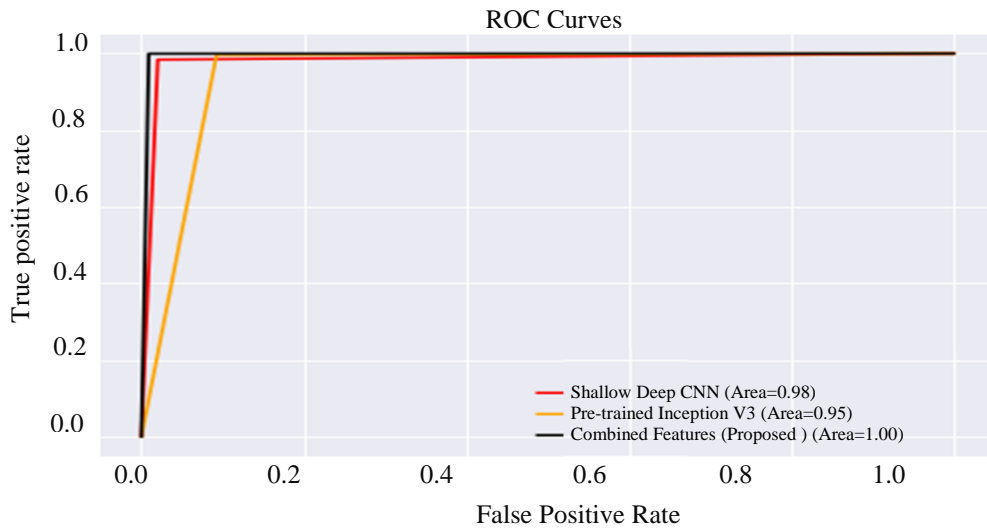**Fig. 10 Comparison of combined features accuracy on the MIAS dataset**

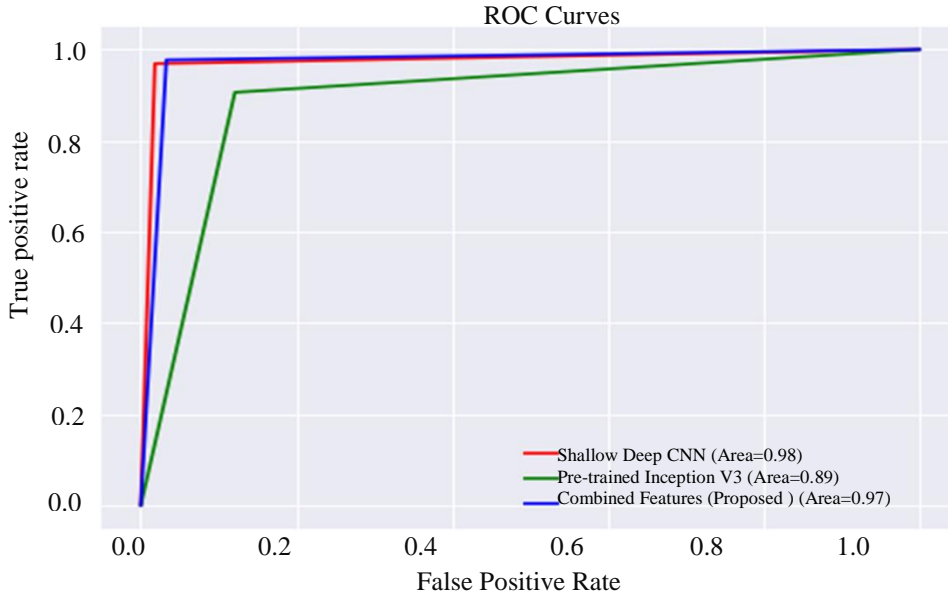**Fig. 11 AUC-ROC comparison for the DDSM + CBIS-DDSM dataset**

Fig. 12 AUC-ROC comparisons for the MIAS dataset

Table 3. Accuracy-based comparative analysis of the proposed hybrid architecture with traditional approaches

Work	Dataset	Techniques	Class Category	Accuracy (%)	AUC
Gnanasekaran et al. [10] (2020)	MIAS DDSM	CNN	3-class (Normal, Benign, Malignant)	92.54 96.47	0.85 0.96
Houby et al. [52] (2021)	INbreast MIAS	CNN	2- class (Malignant, Nonmalignant)	96.52 95.30	0.98 0.974
Ragab et al. [67] (2021)	CBIS-DDSM MIAS	Deep features fusion	2-class (Benign, Malignant) 2-class (Normal, Abnormal)	97.90 97.40	1 1
Karthiga et al. [32] (2022)	MIAS DDSM	Deep CNN and Pre-strained model	2- class (Benign, Malignant)	95.95 99.39	
Kumar et al. [70] 2022	DDSM+CBIS-DDSM	End-to-end CNN	2-class (Normal, Malignant)	97.20	
Proposed hybrid architecture	MIAS DDSM+ CBIS-DDSM	DeepCNN+InceptionV3+ IE-NDR +GI-CDT	2- class (Benign, Malignant) 2-class (Positive, Negative)	97.53 99.52	0.97 1

5. Discussion

We implemented a hybrid CNN architecture to classify breast cancer using mammogram images. The architecture included a shallow, deep CNN, transfer learning, dimensionality reduction, and classification algorithms applied to the DDSM + CBIS-DDSM and MIAS datasets to achieve superior specificity, sensitivity, and accuracy performance. The findings are listed as follows:

1. In the first experiment, we designed a shallow, deep CNN with five convolutional layers, five max-pooling layers, one batch normalization layer, and one dropout layer, which achieved an accuracy of 97% on the DDSM + CBIS-DDSM and MIAS datasets.
2. In the second experiment, we used TL by replacing the last FC layer of the pre-trained Inception-v3 architecture

with a new one for performing binary classification, which resulted in an accuracy of 96% and 89% on the DDSM + CBIS-DDSM and MIAS datasets, respectively.
3. The designed shallow, deep CNN model achieved higher accuracy and required less training time than the pre-trained InceptionV3 model.
4. In the third experiment, we combined the features obtained using the first two experiments and applied IE-NDR to minimize the feature space and complexity of the classification process.
5. We used GI-CDT, which considers all possible outcomes, in the classification process.
6. The combination of features using IE-NDR resulted in accuracy, sensitivity, and specificity of 99.52%, 98%, and 99.63%, respectively, on the DDSM + CBIS-DDSM

dataset and 97.53%, 97%, and 98.05%, on the MIAS dataset.

7. The proposed architecture, which utilized the designed shallow, deep CNN and combined features, achieved higher accuracy on the MIAS dataset than the traditional deep CNN model [10].

8. The proposed architecture yielded an AUC value 1.0 on the DDSM + CBIS-DDSM dataset.

Further research can be conducted to explore different feature extraction techniques in combination with deep learning architectures. Different feature reduction techniques could also be investigated to enhance classification accuracy and feature selection.

6. Conclusion

In this study, we conducted three experiments to classify mammogram images and assess the efficiency of the proposed model using two different mammogram datasets. In the first experiment, we designed a shallow, deep CNN with lower complexity, followed by using a pre-trained Inceptionv3 model in the second experiment, which proved to be faster. In the third experiment, we combined the features extracted by the hybrid shallow, deep CNN and pre-trained Inception-v3 model, using dimensionality reduction IE-NDR. The results indicate that the proposed model attained a high level of accuracy. Specifically, it yielded 99.52% accuracy and 96% AUC on the DDSM + CBIS-DDSM dataset and 97.53% accuracy and 97% AUC on the MIAS dataset. Our system is easy to construct, inexpensive, effective, and automated, and can assist medical professionals, especially radiologists, in analyzing breast cancer from mammograms. The proposed system is expected to reduce the time and energy required for testing and the number of diagnostic errors caused by human exhaustion.

References

[1] Qing Guo et al., "Relationship between Particulate Matter Exposure and Female Breast Cancer Incidence and Mortality: A Systematic Review and Meta-Analysis," *International Archives of Occupational and Environmental Health,* vol. 94, no. 2, pp. 191-201, 2021. [CrossRef][Google Scholar][Publisher Link]

[2] R. L. Siegel, K. D. Miller, and A. Jemal, "Cancer Statistics, 2015," *CA: A Cancer Journal for Clinicians*, vol. 65, no. 1, pp. 5-29, 2015. [CrossRef][Google Scholar][Publisher Link]

[3] L. H. Eaton, N. Narkthong, and J. M. Hulett, "Psychosocial Issues Associated with Breast Cancer-Related lymphedema: A Literature Review," *Current Breast Cancer Reports,* vol. 12, no. 4, pp. 216-24, 2020. [CrossRef][Google Scholar][Publisher Link]

[4] Bharti Thakur, Nagesh Kumar, and Gaurav Gupta, "Machine Learning Techniques with ANOVA for the Prediction of Breast Cancer," *International Journal of Advanced Technology and Engineering Exploration,* vol. 9, no. 87, pp. 232-245, 2022. [CrossRef][Google Scholar][Publisher Link]

[5] Dina A. Ragab et al., "Breast Cancer Detection using Deep Convolutional Neural Networks and Support Vector Machines," *Bioinformatics and Genomics*, vol. 7, pp. 6201, 2019. [CrossRef][Google Scholar][Publisher Link]

[6] Ashutosh Kumar Dubey, Umesh Gupta, and Sonal Jain, "Medical Data Clustering and Classification using TLBO and Machine Learning Algorithms," *Computers, Materials and Continua,* vol. 70, no. 3, pp. 4523-4543, 2022. [CrossRef][Google Scholar][Publisher Link]

[7] Gul Shaira Banu Jahangeer, and T. Dhiliphan Rajkumar, "Early Detection of Breast Cancer using Hybrid of Series Network and VGG-16," *Multimedia Tools and Applications,* vol. 80, no. 5, pp. 7853-86, 2021. [CrossRef][Google Scholar][Publisher Link]

[8] Gelan Ayana, Kokeb Dese, and Se-woon Choe, "Transfer Learning in Breast Cancer Diagnoses via Ultrasound Imaging," *Cancers,* vol. 13, no. 4, pp. 1-15, 2021. [CrossRef][Google Scholar][Publisher Link]

[9] Meha Desai, and Manan Shah, "An Anatomization on Breast Cancer Detection and Diagnosis Employing Multi-Layer Perceptron Neural Network (MLP) and Convolutional Neural Network (CNN)," *Clinical eHealth,* vol. 4, pp. 1-11, 2021. [CrossRef][Google Scholar][Publisher Link]

[10] Vaira Suganthi Gnanasekaran, "Deep Learning Algorithm for Breast Masses Classification in Mammograms," *IET Image Processing,* vol. 14, no. 12, pp. 2860-2868, 2020. [CrossRef][Google Scholar][Publisher Link]

[11] Runyu Song, Taoying Li, and Yan Wang, "Mammographic Classification Based on XGBoost and DCNN with Multi Features," *IEEE Access*, vol. 8, pp. 75011-75021, 2020. [CrossRef][Google Scholar][Publisher Link]

[12] Lizhen Shen et al., "Optimal Breast Tumor Diagnosis using Discrete Wavelet Transform and Deep Belief Network Based on Improved Sunflower Optimization Method," *Biomedical Signal Processing and Control,* vol. 60, 2020. [CrossRef] [Google Scholar] [Publisher Link]

[13] Kristoffersen Edward Mayce R. Lomboy, and Rowell M. Hernandez, "A Comparative Performance of Breast Cancer Classification using Hyper-Parameterized Machine Learning Models," *International Journal of Advanced Technology and Engineering Exploration*, vol. 8, no. 82, pp. 1080-1101, 2021.[Google Scholar] [Publisher Link]

[14] Mehreen Tariq et al., "Medical Image Based Breast Cancer Diagnosis: State of the Art and Future Directions," *Expert Systems with Applications,* vol. 167, 2021. [CrossRef] [Google Scholar] [Publisher Link]

[15] Saeed Talatian Azad, Gholamreza Ahmadi, and Amin Rezaeipanah, "An Intelligent Ensemble Classification Method Based on Multi-Layer Perceptron Neural Network and Evolutionary Algorithms for Breast Cancer Diagnosis," *Journal of Experimental & Theoretical Artificial Intelligence,* vol. 34, no. 6, pp. 949-969, 2022. [CrossRef] [Google Scholar] [Publisher Link]

[16] Vivek Lahoura et al., "Cloud Computing-Based Framework for Breast Cancer Diagnosis using Extreme Learning Machine," *Diagnostics,* vol. 11, no. 2, pp. 1-19, 2021. [CrossRef] [Google Scholar] [Publisher Link]

[17] B. V. Divyashree, and G. Hemantha Kumar, "Breast Cancer Mass Detection in Mammograms using Gray Difference Weight and MSER Detector," *SN Computer Science,* vol. 2, no. 2, pp. 1-3, 2021. [CrossRef] [Google Scholar] [Publisher Link]

[18] V. Nemade et al., "A Review and Computational Analysis of Breast Cancer using Different Machine Learning Techniques," *International Journal of Emerging Technology and Advanced Engineering*, vol. 12, no. 3, pp. 111-118, 2022. [CrossRef] [Google Scholar] [Publisher Link]

[19] Angel Cruz-Roa et al., "Automatic Detection of Invasive Ductal Carcinoma in Whole Slide Images with Convolutional Neural Networks," *SPIE Medical Imaging,* vol. 9041, 2014. [CrossRef] [Google Scholar] [Publisher Link]

[20] Shankar Shambhu et al., "Binary Classification of Covid-19 CT Images using CNN: Covid Diagnosis using CT," *International Journal of E-Health and Medical Communications (IJEHMC),* vol. 13, no. 2, pp. 1-3, 2021. [CrossRef] [Google Scholar] [Publisher Link]

[21] Shadi Albarqouni et al., "Aggnet: Deep Learning from Crowds for Mitosis Detection in Breast Cancer Histology Images," *IEEE Transactions on Medical Imaging*, vol. 35, no. 5, pp. 1313-21, 2016. [CrossRef] [Google Scholar] [Publisher Link]

[22] Jing Zheng et al., "Deep Learning Assisted Efficient AdaBoost Algorithm for Breast Cancer Detection and Early Diagnosis," *IEEE Access*, vol. 8, pp. 96946-96954, 2020. [CrossRef] [Google Scholar] [Publisher Link]

[23] Hau Li et al., "Benign and Malignant Classification of Mammogram Images Based on Deep Learning," *Biomedical Signal Processing and Control,* vol. 51, pp. 347-354, 2019. [CrossRef] [Google Scholar] [Publisher Link]

[24] Yanfeng Lli et al., "Mass Detection in Mammograms by Bilateral Analysis using Convolution Neural Network," *Computer Methods and Programs in Biomedicine,* vol. 195, 2020. [CrossRef] [Google Scholar] [Publisher Link]

[25] Ahmad Firdaus Ahmad Fadzil, Noor Elaiza Abd Khalid, and Shafaf Ibrahim, "Amplification of Pixels in Medical Image Data for Segmentation via Deep Learning Object-Oriented Approach," *International Journal of Advanced Technology and Engineering Exploration*, vol. 8, no. 74, pp. 82-90, 2021. [Google Scholar] [Publisher Link]

[26] Natalia Antropova, Benjamin Q. Huynh, and Maryellen L. Giger, "A Deep Feature Fusion Methodology for Breast Cancer Diagnosis Demonstrated on Three Imaging Modality Datasets," *Medical Physics*, vol. 44, no. 10, pp. 5162-5171, 2017. [CrossRef] [Google Scholar] [Publisher Link]

[27] M. S. Alam Noor et al., "Automated Sheep Facial Expression Classification using Deep Transfer Learning," *Computers and Electronics in Agriculture,* vol. 175, 2020. [CrossRef] [Google Scholar] [Publisher Link]

[28] Bufan Liu et al., "A Cost-Effective Manufacturing Process Recognition Approach based on Deep Transfer Learning for CPS Enabled Shop-Floor," *Robotics and Computer-Integrated Manufacturing,* vol. 70, 2021. [CrossRef] [Google Scholar] [Publisher Link]

[29] Rachna Jain et al., "Pneumonia Detection in Chest X-Ray Images using Convolutional Neural Networks and Transfer Learning," *Measurement,* vol. 165, 2020. [CrossRef] [Google Scholar] [Publisher Link]

[30] Tariq Mahmood et al., "Breast Mass Detection and Classification using Deep Convolutional Neural Networks for Radiologist Diagnosis Assistance," *IEEE Annual Computers, Software, and Applications Conference*, pp. 1918-1923, 2021. [CrossRef] [Google Scholar] [Publisher Link]

[31] Mugahed A. Al-antari, Seung-Moo Han, and Tae-Seong Kim, "Evaluation of Deep Learning Detection and Classification Towards a Computer-Aided Diagnosis of Breast Lesions in Digital X-Ray Mammograms," *Computer Methods and Programs in Biomedicine*, vol. 196, 2020. [CrossRef] [Google Scholar] [Publisher Link]

[32] R. Karthiga, K. Narasimhan, and Rengarajan Amirtharajan, "Diagnosis of Breast Cancer for Modern Mammography using Artificial Intelligence," *Mathematics and Computers in Simulation,* vol. 202, pp. 316-330, 2022. [CrossRef] [Google Scholar] [Publisher Link]

[33] Haibo Wang et al., "Cascaded Ensemble of Convolutional Neural Networks and Handcrafted Features for Mitosis Detection," *Medical Imaging*, vol. 9041, pp. 66-75, 2014. [CrossRef] [Google Scholar] [Publisher Link]

[34] Yang Xin et al., "Machine Learning and Deep Learning Methods for Cyber Security," *IEEE Access,* vol. 6, pp. 35365-35381, 2018. [CrossRef] [Google Scholar] [Publisher Link]

[35] Iqbal H. Sarker, "Deep Learning: A Comprehensive Overview of Techniques, Taxonomy, Applications and Research Directions," *SN Computer Science,* vol. 2, no. 6, pp. 1-20, 2021. [CrossRef] [Google Scholar] [Publisher Link]

[36] Qaisar Abbas, "DeepCAD: A Computer-Aided Diagnosis System for Mammographic Masses using Deep Invariant Features," *Computers*, vol. 5, no. 4, pp. 1-15, 2016. [CrossRef] [Google Scholar] [Publisher Link]

[37] M. A. Al-masni et al., "Detection and Classification of Breast Abnormalities in Digital Mammograms via Regional Convolutional Neural Network," *Annual International Conference of the IEEE Engineering in Medicine and Biology Society,* pp. 1230-1233, 2017. [CrossRef] [Google Scholar] [Publisher Link]

[38] Omar Ibrahim Obaid et al., "Evaluating the Performance of Machine Learning Techniques in Classifying Wisconsin Breast Cancer," *International Journal of Engineering and Technology,* vol. 7, pp. 160-166, 2018.[Google Scholar] [Publisher Link]

[39] Aditya A. Shastri, Deepti Tamrakar, and Kapil Ahuja, "Density-Wise Two Stage Mammogram Classification using Texture Exploiting Descriptors," *Expert Systems with Applications,* vol. 99, pp. 71-82, 2018. [CrossRef] [Google Scholar] [Publisher Link]

[40] Bushra Mughal et al., "A Novel Classification Scheme to Decline the Mortality Rate among Women Due To Breast Tumor," *Microscopy Research and Technique,* vol. 81, no. 2, pp. 171-80, 2018. [CrossRef] [Google Scholar] [Publisher Link]

[41] Ardalan Ghasemzadeh, Saeed Sarbazi Azad, and Elham Esmaeili, "Breast Cancer Detection Based on Gabor-Wavelet Transform and Machine Learning Methods," *International Journal of Machine Learning and Cyberneticsm,* vol. 10, no. 7, pp. 1603-1612, 2019. [CrossRef] [Google Scholar] [Publisher Link]

[42] Mugahed A. Al-antari et al., "A Fully Integrated Computer-Aided Diagnosis System for Digital X-Ray Mammograms via Deep Learning Detection, Segmentation, and Classification," *International Journal of Medical Informatics,* vol. 117, pp. 44-54, 2018. [CrossRef] [Google Scholar] [Publisher Link]

[43] Richa Agarwal et al., "Automatic Mass Detection in Mammograms using Deep Convolutional Neural Networks," *Journal of Medical Imaging,* vol. 6, no. 3, 2019. [CrossRef] [Google Scholar] [Publisher Link]

[44] Prabhpreet Kaur, Gurvinder Singh, and Parminder Kaur, "Intellectual Detection and Validation of Automated Mammogram Breast Cancer Images by Multi-Class SVM using Deep Learning Classification," *Informatics in Medicine Unlocked,* vol. 16, 2019. [CrossRef] [Google Scholar] [Publisher Link]

[45] Figlu Mohanty, Suvendu Rup, and Bodhisattva Dash, "Automated Diagnosis of Breast Cancer using Parameter Optimized Kernel Extreme Learning Machine," *Biomedical Signal Processing and Control,* vol. 62, 2020. [CrossRef] [Google Scholar] [Publisher Link]

[46] DArvin Yi et al., "Optimizing and Visualizing Deep Learning for Benign/Malignant Classification in Breast Tumors," *Computer Vision and Pattern Recognition,* 2017. [CrossRef] [Google Scholar] [Publisher Link]

[47] Dezso Ribli et al., "Detecting and Classifying Lesions in Mammograms with Deep Learning," *Scientific Reports,* vol. 8, no. 1, pp. 1-7, 2020. [CrossRef] [Google Scholar] [Publisher Link]

[48] Hiba Chougrad, Hamid Zouaki, and Omar Alheyane, "Multilabel Transfer Learning for the Early Diagnosis of Breast Cancer," *Neurocomputing,* vol. 392, pp. 168-180, 2020. [CrossRef] [Google Scholar] [Publisher Link]

[49] Xiangchun Yu et al., "Mammographic Image Classification with Deep Fusion Learning," *Scientific Reports,* vol. 10, no. 1, pp. 1-11, 2020. [CrossRef] [Google Scholar] [Publisher Link]

[50] S. R. Sannasi Chakravarthy, and H. Rajaguru, "Automatic Detection and Classification of Mammograms using Improved Extreme Learning Machine with Deep Learning," *IRBM*, vol. 43, no. 1, pp. 49-61, 2022. [CrossRef] [Google Scholar] [Publisher Link]

[51] Xiang Yu, Kaijian Xia, and Yu-Dong Zhang, "Disep Net for Breast Abnormality Recognition," *Computers & Electrical Engineering,* vol. 90, 2021. [CrossRef] [Google Scholar] [Publisher Link]

[52] Enas M. F. El Houby, and Nisreen I. R. Yassin, "Malignant and Nonmalignant Classification of Breast Lesions in Mammograms using Convolutional Neural Networks," *Biomedical Signal Processing and Control,* vol. 70, 2021. [CrossRef] [Google Scholar] [Publisher Link]

[53] Abeer Saber et al., "Using the Transfer-Learning Technique, A Novel Deep-Learning Model for Automatic Detection and Classification of Breast Cancer," *IEEE Access,* vol. 9, pp. 71194-209, 2021. [CrossRef] [Google Scholar] [Publisher Link]

[54] Sharaf J. Malebary, and Arshad Hashmi, "Automated Breast Mass Classification System using Deep Learning and Ensemble Learning in Digital Mammogram," *IEEE Access,* vol. 9, pp. 55312-55328, 2021. [CrossRef] [Google Scholar] [Publisher Link]

[55] Sujata Kulkarni, and Rinku Rabidas, "A Comparative Study of Different Deep Learning Architectures for Benign-Malignant Mass Classification," *In Proceedings of the International Conference on Recent Trends in Machine Learning, IoT, Smart Cities and Applications*, pp. 773-784, 2022. [CrossRef] [Google Scholar] [Publisher Link]

[56] Idowu Sunday Oyetade et al., "Hybridized Deep Convolutional Neural Network and Fuzzy Support Vector Machines for Breast Cancer Detection," *SN Computer Science,* vol. 3, no. 1, pp. 1-4, 2022. [CrossRef] [Google Scholar] [Publisher Link]

[57] Imran Ul Haq et al., "Feature Fusion and Ensemble Learning-Based CNN Model for Mammographic Image Classification," *Journal of King Saud University-Computer and Information Sciences,* vol. 34, no. 6, pp. 3310-3318, 2022. [CrossRef] [Google Scholar] [Publisher Link]

[58] Shobha Gusain, "Modifiable Risk Factors for Breast and Cervical Cancer and Their Association with Sample Characteristics," *SSRG International Journal of Nursing and Health Science*, vol. 6, no. 1, pp. 10-16, 2020. [CrossRef] [Publisher Link]

[59] Subasish Mohapatra et al., "Evaluation of Deep Learning Models for Detecting Breast Cancer using Histopathological Mammograms Images," *Sustainable Operations and Computers,* vol. 3, pp. 296-302, 2022. [CrossRef] [Google Scholar] [Publisher Link]

[60] Essam H. Houssein, Marwa M. Emam, and Abdelmgeid A. Ali, "An Optimized Deep Learning Architecture for Breast Cancer Diagnosis Based on Improved Marine Predators Algorithm," *Neural Computing and Applications*, vol. 34, pp. 1-9, 2022. [CrossRef] [Google Scholar] [Publisher Link]

[61] Md. Nawaj Sharif et al., "Design and Simulation of a Circular Microstrip Patch Antenna for Breast Cancer Diagnosis," *International Journal of Recent Engineering Science*, vol. 7, no. 3, pp. 57-60, 2020. [CrossRef] [Google Scholar] [Publisher Link]

[62] SanaUllah Khan et al., "A Novel Deep Learning Based Framework for the Detection and Classification of Breast Cancer using Transfer Learning," *Pattern Recognition Letters,* vol. 125, pp. 1-6, 2019. [CrossRef] [Google Scholar] [Publisher Link]

[63] E. A. Scuccimarra, "*DDSM Mammography*," version 4, [Online] . Available: https://www.kaggle.com/skooch/ddsm-mammography

[64] [Online] . Available: https://www.kaggle.com/datasets/kmader/mias-mammography

[65] Christian Szegedy et al., "Inception-V4, Inception-Resnet and the Impact of Residual Connections on Learning," *In Thirty-first AAAI Conference on Artificial Intelligence*, vol. 31, no. 1, pp. 4278-4284, 2017. [CrossRef] [Google Scholar] [Publisher Link]

[66] Christian Szegedy et al., "Rethinking the Inception Architecture for Computer Vision," *In Proceedings of the IEEE Conference on Computer Vision and Pattern Recognition*, pp. 2818-2826, 2016.[Google Scholar] [Publisher Link]

[67] Dina A Ragab et al., "A Framework for Breast Cancer Classification using Multi-DCNNs," *Computers in Biology and Medicine,* vol. 131, 2021. [CrossRef] [Google Scholar] [Publisher Link]

[68] Brotobor Deliverance, Edeawe Isaac Osahogie, and Brotobor Onoriode, "Awareness and Practice of Student Nurses on Breast Self-Examination: A Risk Assessment Tool for Breast Cancer," *SSRG International Journal of Nursing and Health Science*, vol. 6, no. 1, pp. 66-69, 2020. [CrossRef] [Publisher Link]

[69] Nidhi Mongoriya, and Vinod Patel, "Review the Breast Cancer Detection Technique using Hybrid Machine Learning," *SSRG International Journal of Computer Science and Engineering*, vol. 8, no. 6, pp. 5-8, 2021. [CrossRef] [Publisher Link]

[70] Pradeep Kumar et al., "End-to-End Improved Convolutional Neural Network Model for Breast Cancer Detection using Mammographic Data," *The Journal of Defense Modeling and Simulation: Applications, Methodology, Technology,* vol. 19, no. 3, 2022. [CrossRef] [Google Scholar] [Publisher Link]